Summary of Supplementary Materials:

1) Materials and Methods.
2) Supplementary tables(a total of eight).
3) Supplementary table descriptions.
4) A movie and movie description.
5) Supplementary figures and descriptions (a total of seven).
6) References for supplementary materials.

Materials and Methods:

Islet cell preparation, scRNA-seq, and DNA methylome assays

*MNYI i*slet isolation and dissociation followed that in Star Method. Details of scRNA-seq data and DNA methylome assays were described in Star-method as well.

Mitochondrial activity assays

For comparing mitochondrial mass and activity, islets from 2-3 month-old *MNYI* mice (both males and females) were isolated and dissociated into single cells. They were then stained with MitoView^{TM} 633 or MitoView^{TM} 650 (Biotium) at 37 °C for 15 minutes in the presence of 20 mM glucose, immediately followed by Flow-cytometry analysis (Ernst et al., 2023). These dyes are used to measure the mitochondrial transmembrane potential and mitochondrial mass, respectively. The β-cells were gated into eYFP^{+} and eYFP^{-} β-cell subtypes in order to compare their MitoView^{TM} signals. For ADP/ATP ratio in purified β-cell subtypes, an EnzyLight^{TM} ADP/ATP ratio Assay Kit (BioAssay Syetems) was used, following the manufacturer's protocols.

Immunofluorescence (IF) assays

IF assays followed routine procedures using frozen sections. Antibodies are listed in reagent table.

Table S8: Genes used to subdivide human β cell.

CHGA	Vesicle production (Wollam et al., 2017)
EEF1A1	Stress-related (Vera et al., 2014)
EIF1	Stress-related (Sehrawat et al., 2022)
GNAS	Secretion (Taneera et al., 2019)
HINT1	Apoptosis regulator (Weiske and Huber, 2006)
HSP90AB1	Stress-related (Haase and Fitze, 2016)
INS	Vesicle production
MT-CO1	Cellular senescence (Kim et al., 2018)
OAZ1	Cell proliferation (Wang and Jiang, 2014)
PCSK1N	Hormone processing (Liu et al., 2012)
PCSK2	Hormone processing (Jonsson et al., 2012)
PEBP1	Cell proliferation (Rajkumar et al., 2016)
RAB11A	Vesicle production (Khandelwal et al., 2008)
RBP4	Stress-related (Zabetian-Targhi et al., 2015)
RPL17	Protein synthesis (Wang et al., 2015)
RPL31	Protein synthesis (Peisker et al., 2008)
SOD1	Stress-related (Xu et al., 2022)
Syt7	Secretion (Wu et al., 2015)
TPD52	Vesicle trafficking (Thomas et al., 2010)
TPT1	Cell death (Ma, 2021)

Movie-S1: An example of real-time imaging of GCaMP6 of a few female MNA islets. Recording interval is 5 seconds. Basal glucose is 1mM. Stimulatory glucose is 11 mM,

Table S1. Numbers of tdT^+ and tdT^- β cells identified by scRNA-seq at P2 and P60. Related to Fig. 2 and 3.

Table S2. DEGs between P2 β-cell subtypes detected by scRNA-seq. The expression level of genes in the 8 samples [4 (S1-S4) tdT^+ and 4 tdT^- cell subtypes] are log-transformed. The average of tdT^+ and tdT^- cells, their difference, p-values are included. Included are also the association between P2 DEGs and P2 DMRs between cell subtypes, both DMRs with lower or higher levels of methylation in $eYFP^+$ cells. Related to Fig. 2 and 5.

Table S3. Pathways/terms/processes that are differentially enriched in P60 β-cell subtypes in males and female mice, respectively. Those indicated by black font are shared between samples of the two sexes (47 out of 55). Those with red font (8 out of 55) are not shared in both sexes. Related to Fig. 3.

Table S4. DEGs between P60 β-cell subtypes detected by scRNA-seq. The expression level of genes in the 12 samples [3 male (M1-M3) tdT^+ and tdT^- subtypes and 3 female (F1-F3) tdT^+ and tdT^- cells] are log-transformed. The average expression levels of tdT^+ and tdT^- cells, their difference, p-values are presented. Also included are the DEGs

that are shared between P2 and P60, those associate with P2 DMRs and P60 DMRs (DMRs with lower and higher levels of methylation are listed in different columns). Related to Figs. 4, 5, and 6.

Table S5. Genes that are associated with DMRs between β-cell subtypes at P2. Three groups of columns are included. They list those associated with DMRs with lower or higher levels of CpG methylation and those associated with both types. Related with Fig. 5. Note that the relative locations of the DMRs to TSS of genes are also included.

Table S6. Genes that are associated with DMRs between β-cell subtypes at P60 and those with both P2 and P60 DMRs. The two column-groups on left list those associated with DMRs with either lower or higher levels of CpG methylation, respectively. The third lists genes that are associate with both P2 and P60 DMRs, with those also displaying differential expression between P60 cell subtypes indicated. Related with Fig. 6. Note that the relative locations of the DMRs to TSS of genes are also included.

Table S7. DEGs in E15.5 endocrine progenitors that are exposed to control and HFD. The FKPMs of DEGs in triplicated samples (HFD and CD) are shown. The fold change was calculated with [(average of HFD) – (average of CD)/average of CD]. P-values were from t-test (two-tails/type 2 errors). Related with Fig. 7.

Table S8. The 20 DEGs between mouse β-cell subtypes that were used for classify human β cells. The references that support the stated roles of genes are provided here.

added at 5 minutes after the recording started. The images used for identification of tdT^- and tdT^+ cells are presented in Fig. S3D.

Supplemental Figures:

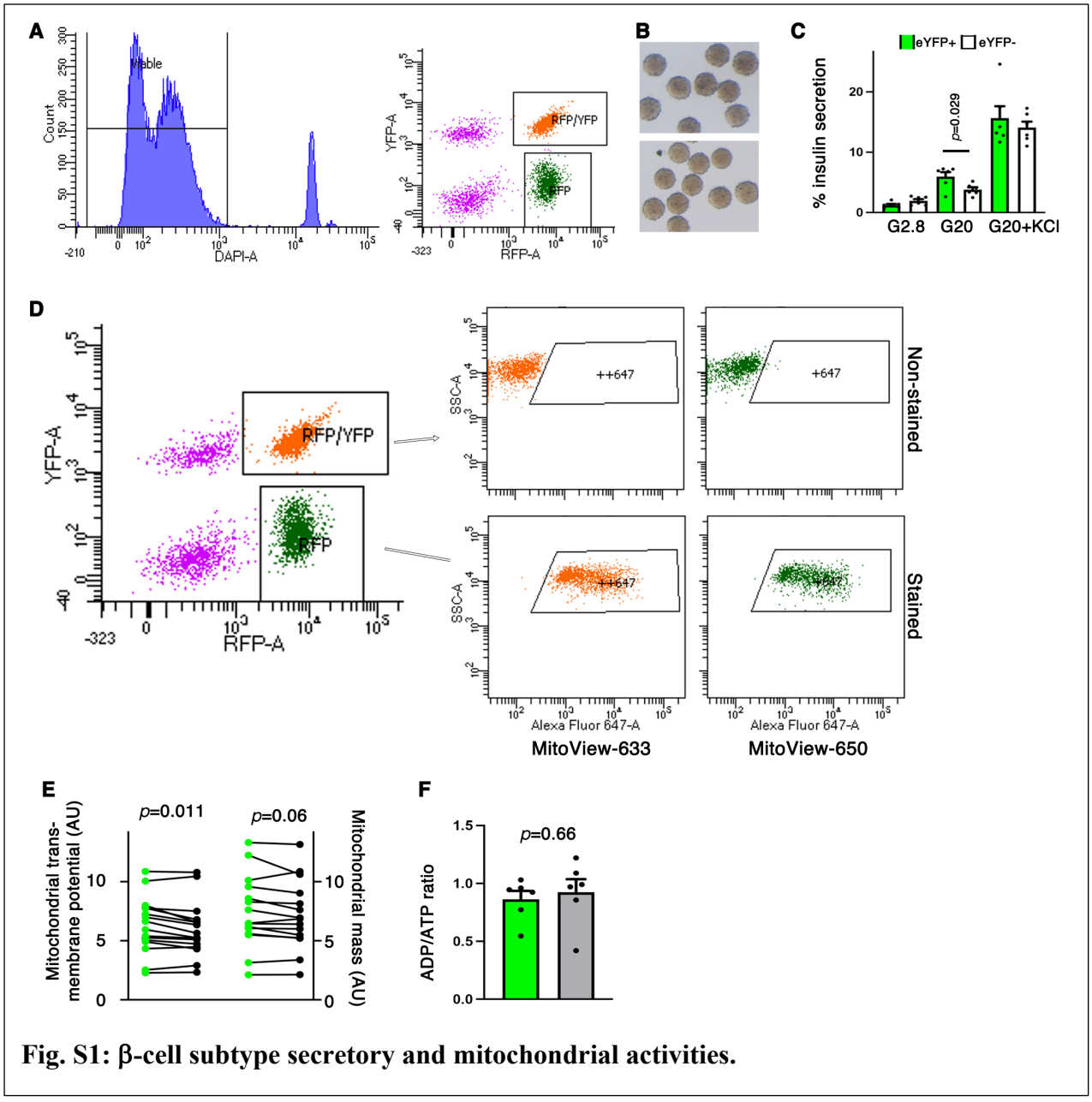

Fig. S1: β-cell subtype secretory and mitochondrial activities.

Fig. S1. Characterization of β-cell subtypes derived from Myt1^{+}Ngn3^{+} (M^{+}N^{+}) and M^{-}N^{+} progenitors in *MNYI* mice. (A) Cell sorting profiles, showing the selection of live cells and those do or do not express *eYFP* (descendants of M^{+}N^{+} and M^{-}N^{+} progenitors, respectively). Note that Apple fluorescent protein is expressed in *Ins^{Apple}* mice, identifying β cells. (B) Typical recovered pseudo-islets (top, eYFP^{+}. Bottom, eYFP^{-}). (C) GSIS from eYFP^{+} or eYFP^{-} pseudo-islets made from MNYI islet cells, with both male and female cells included. The % of total insulin secreted within a 45 minutes time window was presented, as (mean + SEM). *p* value is from unpaired t-test (2-tail type 2 errors). (D) Mitochondrial transmembrane potential and mitochondrial mass assays using MitoView^{TM}633 and MitoView^{TM}650 as indicators, respectively. (E) Quantification of mitochondrial transmembrane potential and mass from flow cytometry assays. (F) ADP/ATP ratios of eYFP^{+} and eYFP^{-} β-cell subtypes from 2-3 months old MNYI mice. Related to Fig. 1.

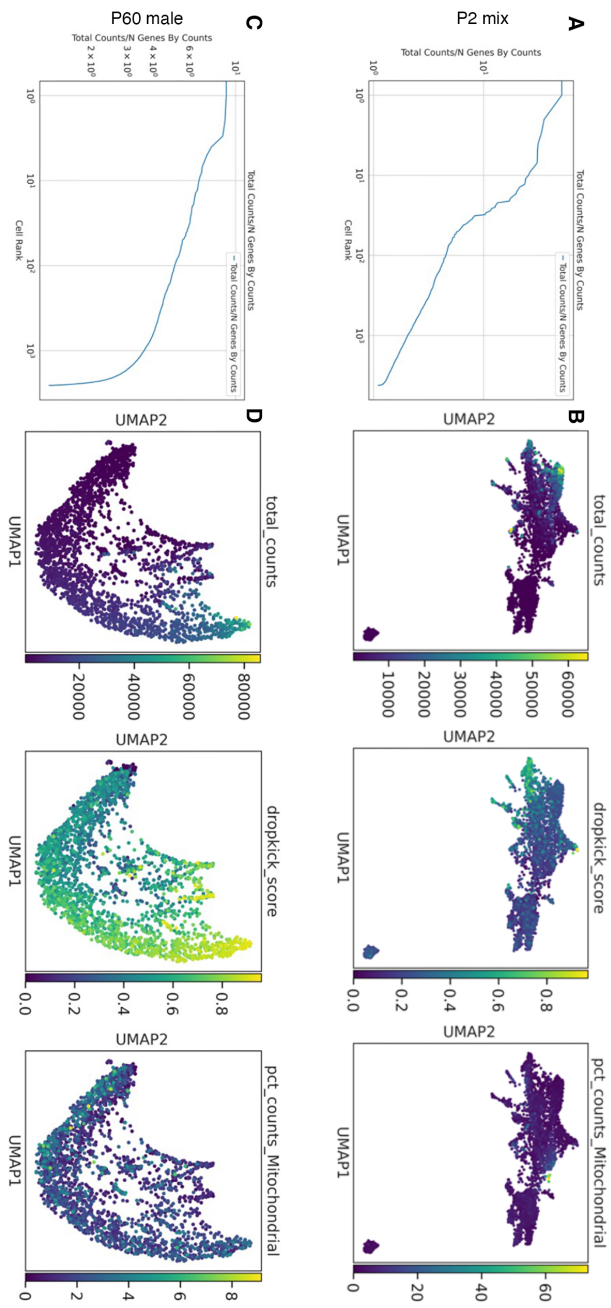

Fig. S2: Quality controls for scRNA-seq.

Fig. S2. Quality controls for scRNA-seq in P2 and P60 β cells. Related to Fig. 2 and 3. (A) An example of cell ranking (based on the total number of count/gene) in P2 islet cells. (B) More detailed quality controls using different criterions (from left to right: total counts per cell, a dropkick algorism that removes poor quality cells, and normalized count over mitochondrial genes that removes dead cells). (C, D) An example of quality control for a P60 male islet samples. The layout follows that of P2.

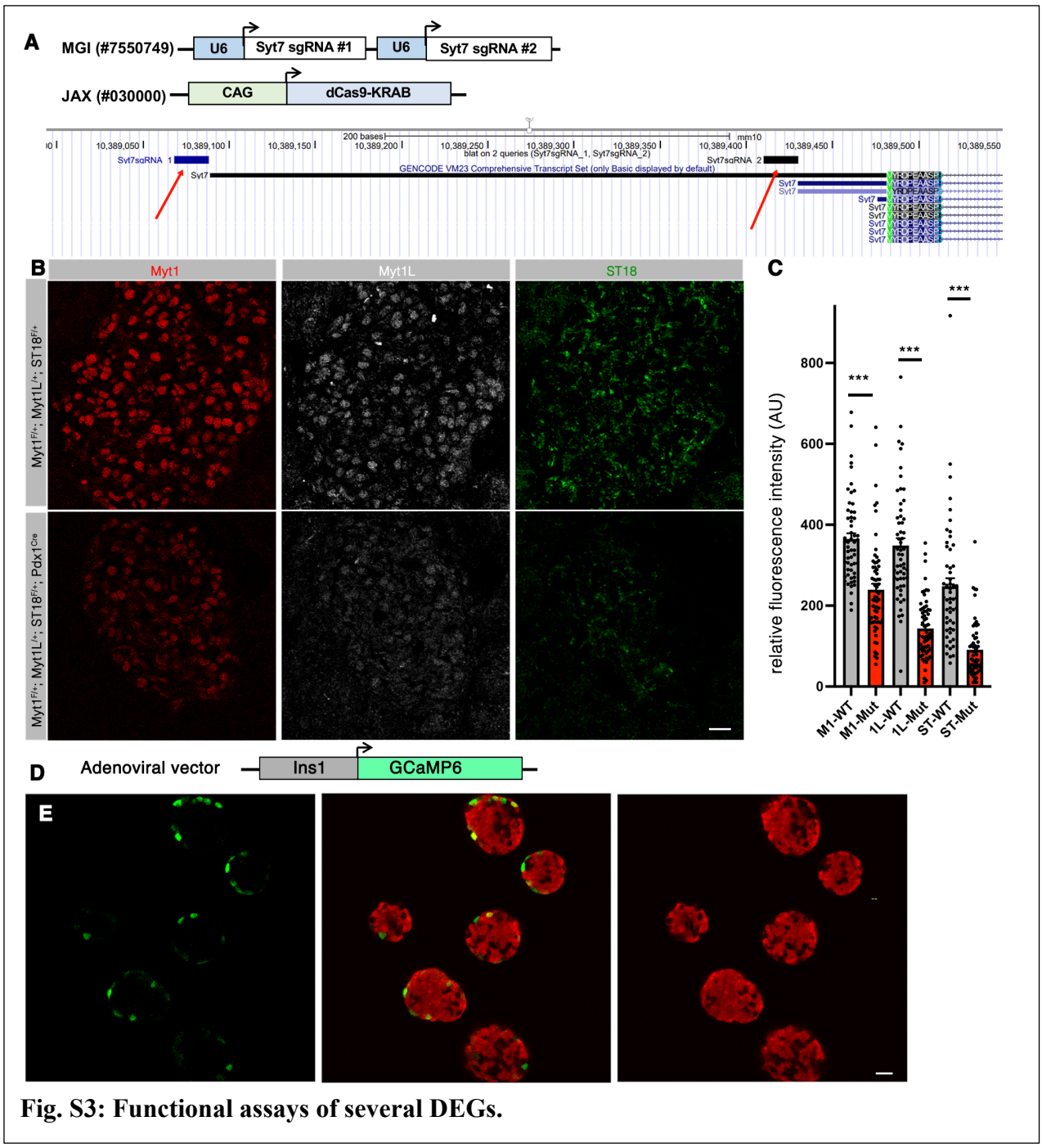

Fig. S3: Functional assays of several DEGs.

Fig. S3. Gene dosage manipulation and β-cell labeling with GCaMP6. Related to Fig. 4. (A) The transgene used for *Syt7* transcriptional repression based on CRSPRi (top). The locations of the two guide RNAs were marked (red arrows), in reference to the two transcriptional starting sites. (B, C) Immunofluorescence (IF) assays of Myt1 (M1), Myt1L (1L), and St18 (ST) levels in islets of P21 heterozygous mice. Shown in (C) are the average IF intensity per islet area (artificial units or AU). Each dot is one islet section, with 3 mice of each genotype used. ***: p<0.001, t-test. Totals between 54-64 sections were used. (D) The construct used to express GCaMP6 specifically in β cells, using adenoviral vector for delivery. (E) Still images of the MNA islet used for GCaMP6 recording, shown in Movie S1. The

isolated islets were infected with adeno viral that drive the expression of GCaMP6 with a Ins1 promoter/enhancer. Bars = 20 μm.

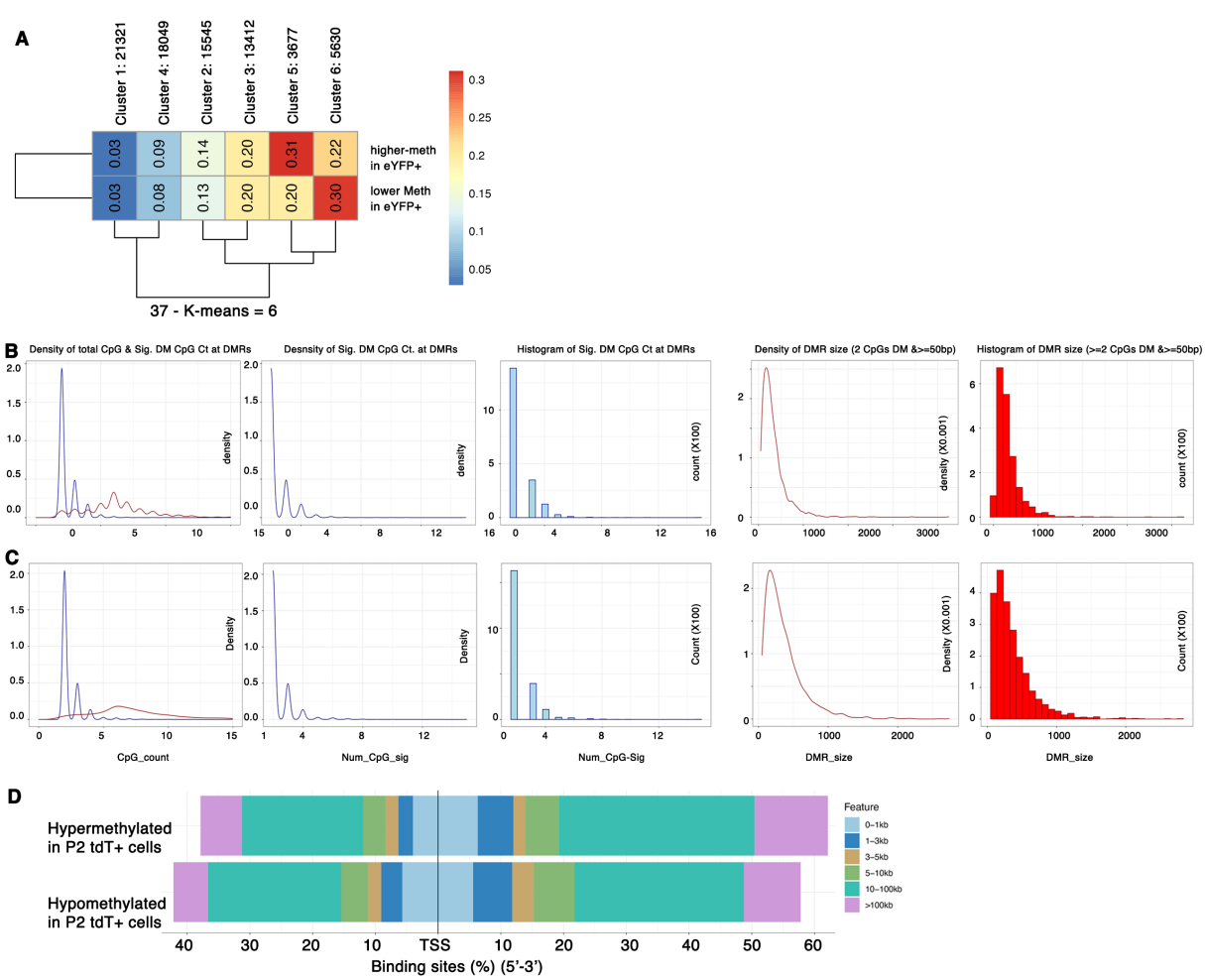

Fig. S4: HMRs and DMRs in P2 β-cell subtypes.

Fig. S4. Identification of HMRs and DMRs between P2 β-cell subtypes. Related to Fig. 5. (A) Clustering of all HMRs identified in P2 eYFP$^+$ and eYFP$^-$ β cell subtypes (from *MNYI* mice). (B, C) Properties of DMRs that have higher (A) or lower methylation levels in DMRs between M$^+$N$^+$ progenitor-derived β-cell subtypes. The properties, from left panel to right are: (1) the density of total number of CpG dinucleotides (red line) and significantly (sig.) demethylated (DM) CpG counts (Ct, blue line) at all the identified DMRs; (2) density of significantly demethylated CpGs at all the DMRs; (3) histogram of significantly demethylated CpGs at all DMRs; (4) Density of DMR size, and (5) histogram of DMR size). (D) The relative locations of DMRs and their putative associated genes, in terms of their location to different features (promoter, intron, exon, intergenic regions, and etc.) of each gene ant their physical distance.

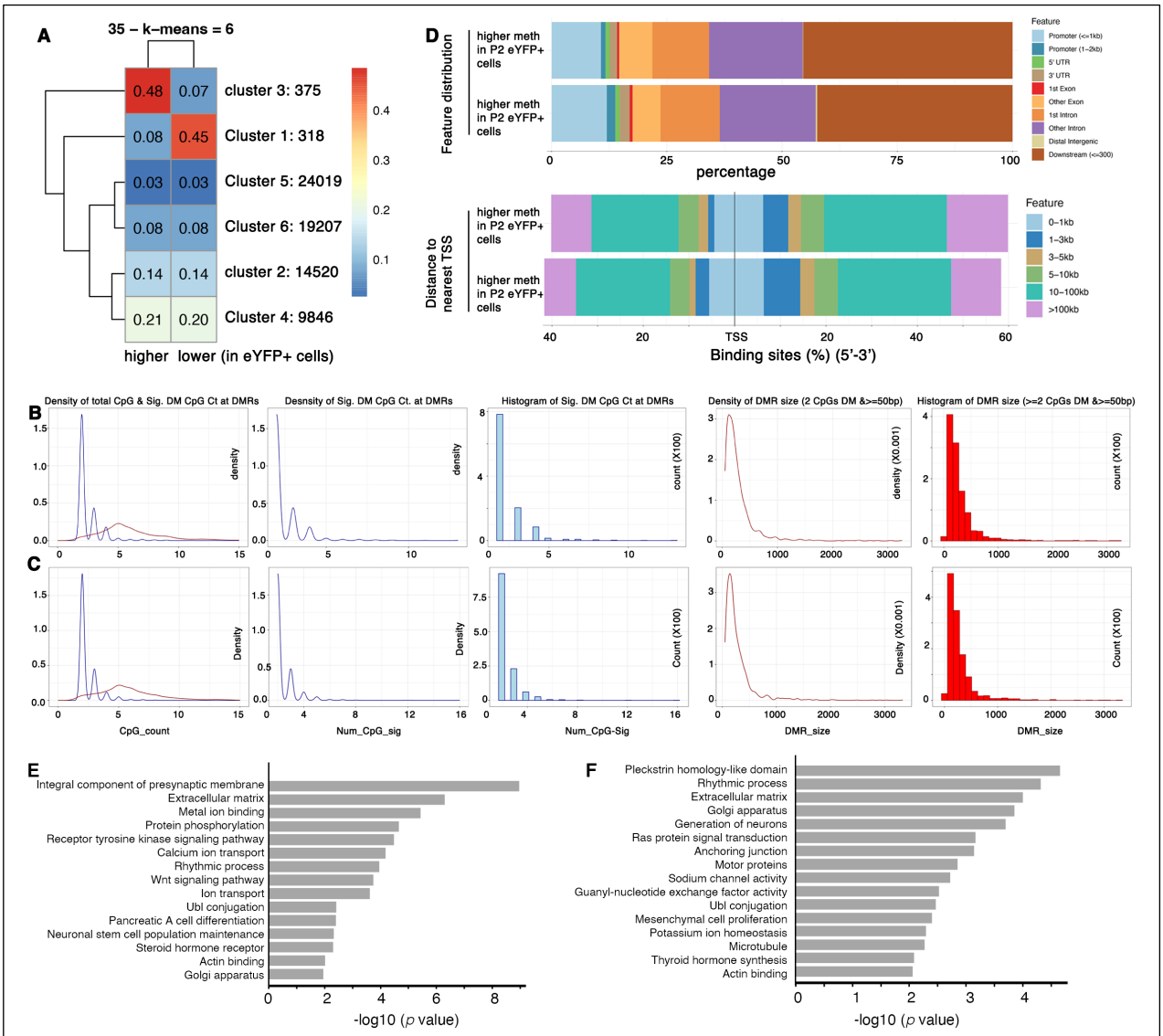

Fig. S5: DNA methylation in P60 β cells.

Fig. S5. Identification of DMRs between P60 β-cell subtypes. (A) Clustering of all HMRs identified in P6 eYFP^{+} and eYFP^{-} β cell subtypes (from *MNYI* mice). (B, C) Properties of DMRs that have higher (B) or lower (C) methylation levels in DMRs between M^{+}N^{+} progenitor-derived β-cell subtypes. The properties, from left panel to right are: (1) the density of total number of CpG dinucleotides (red line) and significantly (sig.) demethylated (DM) CpG counts (Ct, blue line) at all the identified DMRs; (2) density of significantly demethylated CpGs at all the DMRs; (3) histogram of Sig. DM CpGs at all DMRs; (4) Density of DMR size, and (5) histogram of DMR size). (D) The relative locations of DMRs and their putative associated genes, in terms of their location to different features (promoter, intron, exon, intergenic regions, and etc.) of each gene ant their physical distance. (E, F) Terms of genes that are associated with DMRs that have higher (E) or lower (F) levels of DNA methylation in eYFP^{+} β cell subtypes. Related to Fig. 6.

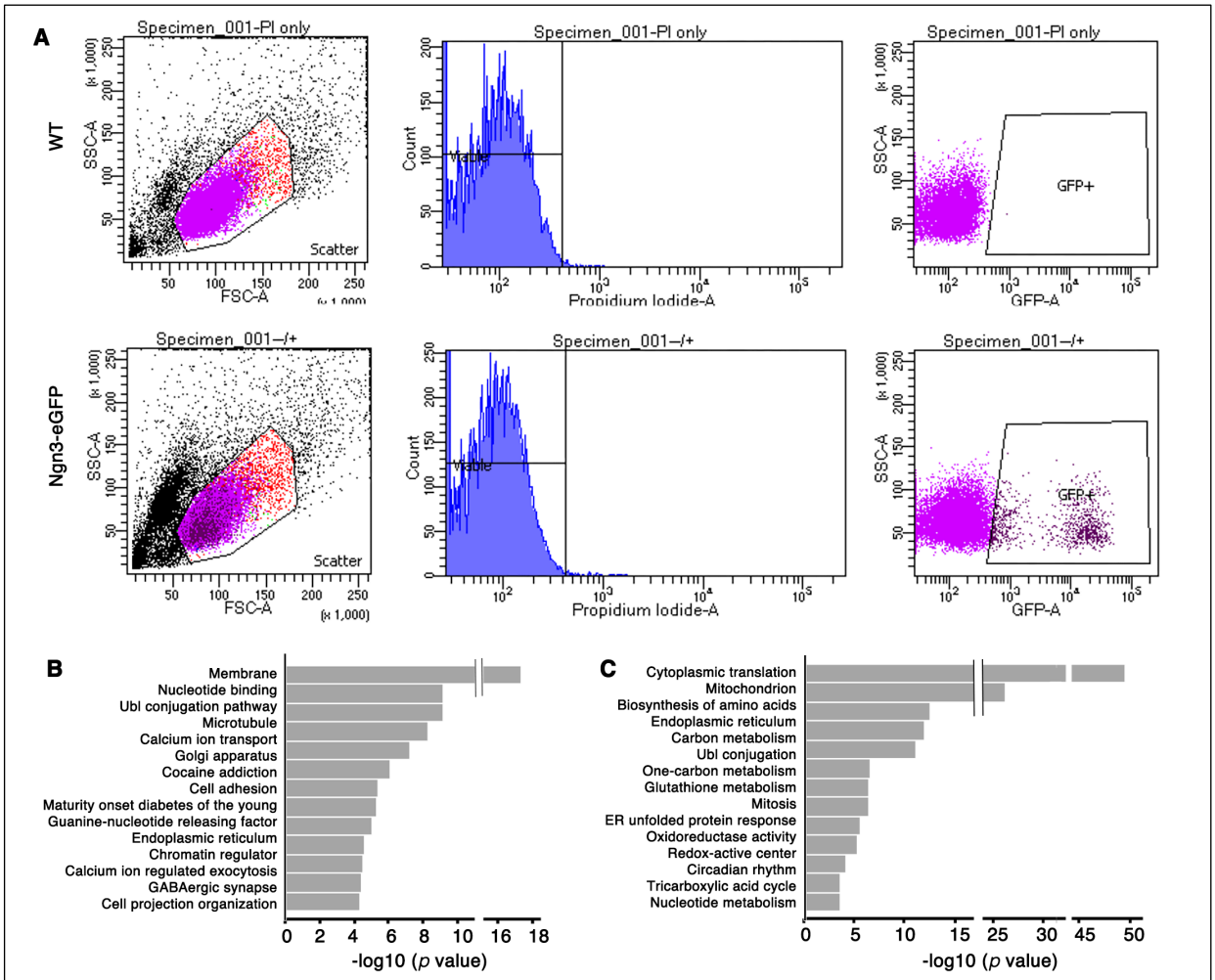

Fig. S6: Purification and expression analysis of E15.5 endocrine progenitors using Ngn3-eGFP mice.

Fig. S6. Purification of E15.5 endocrine progenitors. Related to Fig. 7. (A) FACS gating used to purify the eGFP^{+} islet progenitors from *Neurog3^{eGFP}* mice. (B, C) Biological processes that are down- (A) or up-regulated (B) in endocrine progenitor cells exposed to HFD.

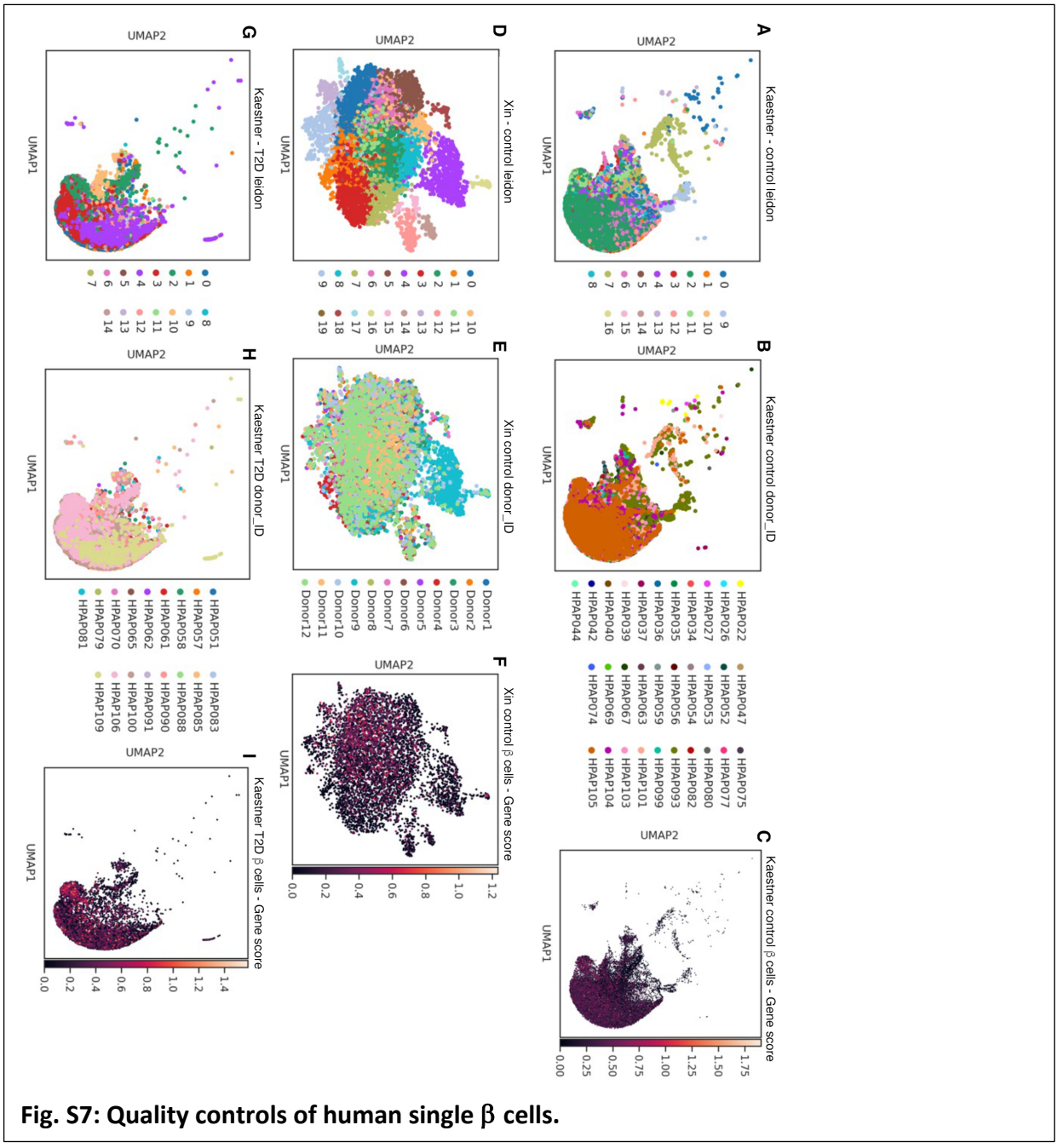

Fig. S7: Quality controls of human single β cells.

Fig. S7. Quality controls for scRNA-seq data analysis of human donor islets. Related to Fig. 7. (A - C) Cell clustering using different algorisms (A, leidon). Overlapped cells from ID-ed donors (B, showing variabilities amongst donors), and gene score (C, used in figures). Panels (D-F) and (G-I) are similar to (A-C), except different islets preps were used.

References

Haase, M., Fitze, G., 2016. HSP90AB1: Helping the good and the bad. Gene 575, 171-186.

Jonsson, A., Isomaa, B., Tuomi, T., Eriksson, J.G., Groop, L., Lyssenko, V., 2012. Effect of a common variant of the PCSK2 gene on reduced insulin secretion. Diabetologia 55, 3245-3251.

Khandelwal, P., Ruiz, W.G., Balestreire-Hawryluk, E., Weisz, O.A., Goldenring, J.R., Apodaca, G., 2008. Rab11a-dependent exocytosis of discoidal/fusiform vesicles in bladder umbrella cells. Proceedings of the National Academy of Sciences of the United States of America 105, 15773-15778.

Kim, S.J., Mehta, H.H., Wan, J., Kuehnemann, C., Chen, J., Hu, J.F., Hoffman, A.R., Cohen, P., 2018. Mitochondrial peptides modulate mitochondrial function during cellular senescence. Aging (Albany NY) 10, 1239-1256.

Liu, T., Zhao, Y., Tang, N., Feng, R., Yang, X., Lu, N., Wen, J., Li, L., 2012. Pax6 directly down-regulates Pcsk1n expression thereby regulating PC1/3 dependent proinsulin processing. PLoS One 7, e46934.

Ma, Y., 2021. Tpt1 the balance toward immunosuppression upon cell death. Nat Immunol 22, 940-942.

Peisker, K., Braun, D., Wolfle, T., Hentschel, J., Funfschilling, U., Fischer, G., Sickmann, A., Rospert, S., 2008. Ribosome-associated complex binds to ribosomes in close proximity of Rpl31 at the exit of the polypeptide tunnel in yeast. Mol Biol Cell 19, 5279-5288.

Rajkumar, K., Nichita, A., Anoor, P.K., Raju, S., Singh, S.S., Burgula, S., 2016. Understanding perspectives of signalling mechanisms regulating PEBP1 function. Cell Biochem Funct 34, 394-403.

Sehrawat, U., Haimov, O., Weiss, B., Tamarkin-Ben Harush, A., Ashkenazi, S., Plotnikov, A., Noiman, T., Leshkowitz, D., Stelzer, G., Dikstein, R., 2022. Inhibitors of eIF4G1-eIF1 uncover its regulatory role of ER/UPR stress-response genes independent of eIF2alpha-phosphorylation. Proceedings of the National Academy of Sciences of the United States of America 119, e2120339119.

Taneera, J., Dhaiban, S., Mohammed, A.K., Mukhopadhyay, D., Aljaibeji, H., Sulaiman, N., Fadista, J., Salehi, A., 2019. GNAS gene is an important regulator of insulin secretory capacity in pancreatic beta-cells. Gene 715, 144028.

Thomas, D.D., Frey, C.L., Messenger, S.W., August, B.K., Groblewski, G.E., 2010. A role for tumor protein TPD52 phosphorylation in endo-membrane trafficking during cytokinesis. Biochem Biophys Res Commun 402, 583-587.

Vera, M., Pani, B., Griffiths, L.A., Muchardt, C., Abbott, C.M., Singer, R.H., Nudler, E., 2014. The translation elongation factor eEF1A1 couples transcription to translation during heat shock response. Elife 3, e03164.

Wang, M., Parshin, A.V., Shcherbik, N., Pestov, D.G., 2015. Reduced expression of the mouse ribosomal protein Rpl17 alters the diversity of mature ribosomes by enhancing production of shortened 5.8S rRNA. RNA 21, 1240-1248.

Wang, X., Jiang, L., 2014. Effects of ornithine decarboxylase antizyme 1 on the proliferation and differentiation of human oral cancer cells. Int J Mol Med 34, 1606-1612.

Weiske, J., Huber, O., 2006. The histidine triad protein Hint1 triggers apoptosis independent of its enzymatic activity. J Biol Chem 281, 27356-27366.
Wollam, J., Mahata, S., Riopel, M., Hernandez-Carretero, A., Biswas, A., Bandyopadhyay, G.K., Chi, N.W., Eiden, L.E., Mahapatra, N.R., Corti, A., Webster, N.J.G., Mahata, S.K., 2017. Chromogranin A regulates vesicle storage and mitochondrial dynamics to influence insulin secretion. Cell Tissue Res 368, 487-501.
Wu, B., Wei, S., Petersen, N., Ali, Y., Wang, X., Bacaj, T., Rorsman, P., Hong, W., Sudhof, T.C., Han, W., 2015. Synaptotagmin-7 phosphorylation mediates GLP-1-dependent potentiation of insulin secretion from beta-cells. Proceedings of the National Academy of Sciences of the United States of America 112, 9996-10001.
Xu, J., Su, X., Burley, S.K., Zheng, X.F.S., 2022. Nuclear SOD1 in Growth Control, Oxidative Stress Response, Amyotrophic Lateral Sclerosis, and Cancer. Antioxidants (Basel) 11.
Zabetian-Targhi, F., Mahmoudi, M.J., Rezaei, N., Mahmoudi, M., 2015. Retinol binding protein 4 in relation to diet, inflammation, immunity, and cardiovascular diseases. Adv Nutr 6, 748-762.